Bistable Buckled Beam: Modeling of Actuating Force and Experimental Validations

Paul Cazottes, Amâncio Fernandes, Joël Pouget, Moustapha Hafez

Bistable Buckled Beam: Modelling of Actuating Force and Experimental Validations

Paul Cazottes[1,2]
[1] UPMC Univ Paris 06, CNRS-UMR 7190,
Institut Jean Le Rond d'Alembert, F-75005 Paris, France
[2]CEA List, Laboratoire d'Interfaces Sensorielles,
F-92265 Fontenay-aux-Roses, France
Email: cazottes@lmm.jussieu.fr

Amâncio Fernandes
UPMC Univ Paris 06, CNRS-UMR 7190,
Institut Jean Le Rond d'Alembert, F-75005 Paris, France
Email: amancio.fernandes@upmc.fr

Joël Pouget
UPMC Univ Paris 06, CNRS-UMR 7190,
Institut Jean Le Rond d'Alembert, F-75005 Paris, France
Email: pouget@lmm.jussieu.fr

Moustapha Hafez
CEA List, Laboratoire d'Interfaces Sensorielles,
F-92265 Fontenay-aux-Roses, France
Email: moustapha.hafez@cea.fr

Compliant bistable mechanisms are a class of mechanical systems that benefit from both compliance, allowing easy manufacturing on a small scale, and bistability, which provides two passive and stable positions. These properties make them first-class candidates not only for micro-switches but also several other robotic appliances.

This paper investigates the actuation of a simple bistable mechanism, the bistable buckled beam. It is pointed out that the position of the actuation has a significant impact on the behaviour of the system. A new model is proposed and discussed, with experimental validations to compare central and offset loading, highlighting the strengths of each.

Introduction

Bistable mechanisms are systems which use deflection to store and release energy in order to obtain two distinct stable positions. They can keep these two separate states without actuation. They can also withstand small disturbances around their stable states, which allows for robust designs. All these properties make them very good candidates for systems which require two working states, for example *on/off*, *open/closed*...

Bistable systems are commonly used as switches [4] in a wide range of sizes from the macro to the micro-world [13]. They are also greatly used in microrobotic applications such as microgrippers or binary robotic devices [3].

Another potential application is quasi-tactile display with a high density matrix of tiny actuators. A spatial resolution of around 1 mm is required to achieve efficient tactile rendering.

When miniaturizing these systems, classical assembly-based mechanisms are very difficult to build. Compliant mechanisms have proved to be a good solution for miniaturization of bistable systems [6]. The actuation technology should be accurately selected. Electromagnetic motors, for example, are difficult to machine and manufacture, and they are oversized in comparison with the whole mechanism. Bilayers, thermal actuators or electrostatic actuators are an example of other common microactuators. Other actuators, called smart materials, look very promising. These materials are said to be *smart* because they are able to react to a modification of their environment. For instance, shape memory alloys (SMA) are able to react to temperature changes, the effect is based on an internal microstructure (Austen-

ite/Martensite) modification. Piezoelectric materials suffer elastic deformations when an electrical field is applied.

This means that by modifying a physical parameter locally, deflection and hence mechanical work can occur. These actuators are of value in the micro-world because as they are made of a single material, they are monolithic. No assembling process is required.

One drawback associated with smart materials is that when we remove the applied power, they tend to come back to their initial state (with some exceptions due to viscosity). Therefore, they need to be continuously powered. For a two-function system, this means that continuous powering is needed. A better design would only be powered during the transition phase between one stable position and the other. We propose to combine a bistable mechanism with a smart actuator giving us a system that can be actuated with much lower power requirements.

Different smart materials cover a large range of deflection and displacement. This allows us to choose between a wide variety of actuation designs. For instance, some actuators will have bending deflection (SMA [14], piezoelectrics, Electro-Active Polymers [10]). Others, such as wire SMAs, will have linear deflection. A force actuation can also be achieved, for instance, with a bender actuator (such as an SMA bender [2]). These kinds of actuators are widespread among smart materials. They are less powerful than their stack equivalents but allow much larger displacements.

In the present paper, we will focus on the actuation of a bistable mechanism using a localized force.

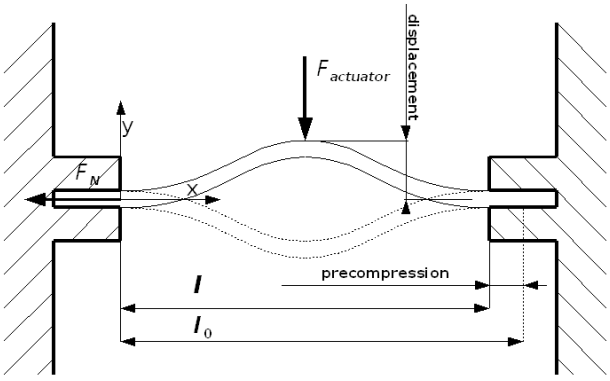

Figure 1. A clamped-clamped bistable mechanism. A force allows the system to snap from one stable position to the other one.

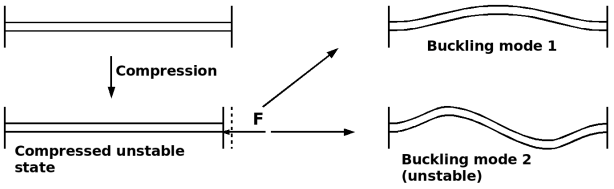

Figure 2. Compression of the beam. The first buckling mode appears. During actuation, the second unstable mode appears.

1 Bistability of precompressed beams

There are two main families of buckled systems. First, mechanisms which are buckled due to lateral force or stress remaining during their manufacturing process. Then, there are systems which are machined with a curved shape [7]. The latter are very accurate for monolithic cuts and can achieve asymmetrical bistability.

A precompressed buckled beam, shown in Fig. 1, is studied in this paper, with different actuation scenarios. The aim is to understand the influence of the actuator location on the performances of the system. This beam is actuated to switch from one stable state to another. A force is applied to the beam at different locations. The resulting displacement of the actuation point along the y axis is determined.

As shown in Fig. 2, the beam is initially straight. It is then shortened by a small percentage of its length at the right end. As predicted by the Euler model, under axial compression greater than a critical force, the beam will buckle in its first buckling mode. A second buckling mode is predicted but will never occur because of its instability (a consequence of a higher level of energy).

The previous analysis can be reproduced for the system with an actuation. A virtual beam, defined as an Euler-Bernoulli beam with no compression energy, can be used to determine the deflection of the beam which will bring an equilibrium solution. The buckling phenomenon is then taken into account to obtain the actual deflection of the system; this means that the deflection can be written as the sum of a general solution (consisting of the first buckling modes) and a particular solution as found before. In the case of the small deflection hypothesis, only the first two buckling modes are considered. The second buckling mode, which does not exist if no forces are applied, may appear thanks to the extra energy brought by the actuation.

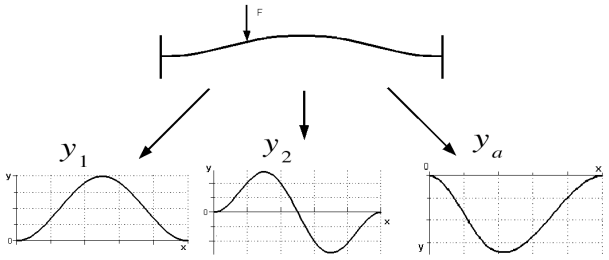

Figure 3. Topological decomposition of the deflection, using a general solution (mode 1, mode 2) and a particular solution.

Previous works for central actuation as [12] or [8] use an energy method, based on the fundamental Euler-Bernoulli beam equations. The internal energy of the system is analytically defined then derived to produce the equilibrium configurations. This could lead to very complex equations if a high degree of precision is desired (hence a large number of buckling modes). To solve it, an analysis of the modes involved makes it possible to reduce the behaviour to two mechani-

cal branches, mode 1 deflection only and mode 2 buckling giving the *N-shape* as defined below. This gives excellent results for central actuation and we present no new results in this regard since our method produces the same results.

However, it is not possible to use the previous analysis for a non-central actuation since the branches are not the same. This paper presents a novel approach, still based on energy, but using a different way of solving the beam equations of bistable systems.

The present analysis, as shown before and represented in Fig. 2 and Fig. 3, makes it possible to split the resolution into two steps. The first is the particular solution resolution, which solves the system before buckling, making it possible to obtain a large number of modes since the deflection is proportional to the actuation excitation and no cross coefficients appear. Next, the buckling phenomena are taken into account through the use of a complex compression equation which has cross parameters. This second resolution is limited to the first two modes as they are topologic so it is possible to solve it speedily with a modern computer and a numerical solver.

These two steps make it possible to benefit from both a high degree of precision (with a large number of modes in the particular shape) and efficient resolution with the only two topologic modes taken into account in the second step. Moreover, it gives the desired equilibrium *f-d* curve directly after the resolution without needing to add and superimpose several mechanical branches in the case of central or shifted actuation.

2 Analytical Model of a Buckled Beam

The system is considered using an out-of-plane beam model. The Euler-Bernoulli beam model was selected. The beam is made of stainless steel, so the deflection will be small enough to ensure that no plastification occurs. The end-shortening was chosen small (2%), so the small-deflection hypothesis is still valid.

2.1 Equation of the buckled beam

The solution for the total deflection is written based on a topological approach as illustrated in Fig. 3. The deflection is the sum of a general solution (for buckling behaviour, including the first and second modes of buckling) and a particular solution (for equilibrium).

Buckling mode 1 is defined by the equations of Euler-Bernoulli for an elastic buckled beam. For a clamped-clamped system, it is given by [11]

$$y_1 = a_1 \left(1 - \cos\left(2\pi \frac{x}{l}\right)\right). \tag{1}$$

For the mode 2, the deflection is given by

$$y_2 = a_2 \left(1 - \frac{2x}{l} - \cos\left(N_2\pi\frac{x}{l}\right) + \frac{2}{N_2\pi}\sin\left(N_2\pi\frac{x}{l}\right)\right) \tag{2}$$

with N_2 the first positive solution for N in the following equation

$$\tan\left(\frac{N}{2}\right) = \frac{N}{2}. \tag{3}$$

The role of those two functions is very different. Buckling mode 1 is responsible for bistability, with the selected state (position 1 or position 2) given by the sign of a_1. On the other hand, buckling mode 2 has no effect on the state and occurs to limit the energy needed to switch from one state to the other. In some cases, this second buckling deflecting never occurs.

Deflection mode 1 and mode 2 are drawn in Fig. 4.

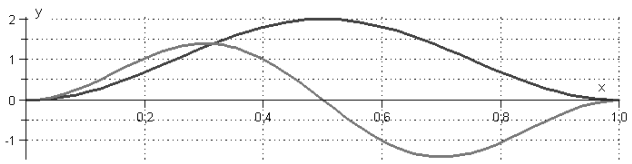

Figure 4. First and second modes of buckling for a clamped-clamped beam. These first two modes coexist during the snapping process.

The particular solution corresponds to an equilibrium solution. It can be determined analytically. Another method, used in this study, is to calculate a particular solution for a virtual beam which has no compression energy using a Galerkin method.

Finally, as y_a is a particular solution due to the actuation force, the deflection is written as

$$y = y_1 + y_2 + y_a. \tag{4}$$

If there are several actuators, several particular solutions must be summed and the deflection becomes

$$y = y_1 + y_2 + \sum_{j=1}^{M} y_a^{(j)} \tag{5}$$

where j is the index of the actuator and M is the total number of actuators.

The displacement of a point P of axial coordinate x_p is given by

$$d = y(x_p). \tag{6}$$

2.2 Energy Relations for a Buckled Beam

The energy of the system is now calculated. An explicit formulation of the energy is used making it possible to draw the energy functions. There are three kinds of energy in the Euler-Bernoulli model.

(i) Bending energy U_b is given by

$$U_b = \int_0^l \frac{EI}{2} \left(\frac{\partial \theta(s)}{\partial s} \right)^2 ds \tag{7}$$

where E is Young's modulus, I the quadratic moment, s the curvilinear coordinate along the beam and θ, the cross-section rotation. If Cartesian axes are used, with a straight beam with small displacements and with E and I constant along the beam, this expression can be approximated by

$$U_b \simeq \frac{EI}{2} \int_0^l y''(x)^2 \, dx. \tag{8}$$

Using Eq. (4), the above energy is then a polynomial function of second order with respect to amplitudes a_1 and a_2.

(ii) Compression energy is calculated using the Hooke law, let us define the deformation as

$$\varepsilon = \frac{\bar{s} - l_0}{l_0} \tag{9}$$

where l_0 is the length of the unladen beam and $\bar{s}$ is the length of the buckled beam given by

$$\bar{s} = \int_0^l ds = \int_0^l \sqrt{1 + y'(x)^2} \, dx. \tag{10}$$

As a small displacement hypothesis is used, an asymptotic development of the square root can be performed, leading to

$$\bar{s} \simeq l + \frac{1}{2} \int_0^l y'(x)^2 \, dx. \tag{11}$$

The cross sectional area S (with $S = bh$) is then used to obtain the compression energy U_c as

$$U_c = \frac{1}{2} SE \varepsilon^2. \tag{12}$$

The result is a polynomial function of the fourth order with respect to amplitudes a_1 and a_2.

The normal force F_N, as shown in Fig. 1 is defined as

$$F_N = SE\varepsilon. \tag{13}$$

(iii) The energy resulting from the external force U_F is the opposite of the work of that force, it is written as

$$U_F = -F \, y(x_F) \tag{14}$$

where F is the force and x_F is the position of the applied force.

Finally, the total energy U_{tot} of the system is the sum of all the previous energies.

$$U_{tot} = U_b + U_c + U_F. \tag{15}$$

2.3 Determination of a Particular Solution

In order to obtain the particular solution y_a, a projection on the buckling modes, as defined in [11], is used. On setting $X = \frac{x}{l}$, the buckling modes are given by

$$y_i = a_i (1 - \cos(N_i X)) \tag{16}$$

for odd i, with $N_i = i\pi$, $i \in \{2, 4...\}$, and

$$y_i = a_i \left(1 - \cos(N_i X) - \frac{2}{N_i} (N_i X - \sin(N_i X)) \right) \tag{17}$$

for even i, with N_i the ith solution to Eq. (3).

The particular solution can be approximated by the first M buckling modes. We take $M = 20$ in order to obtain a good enough accuracy.

$$y_a \simeq \sum_{k=1}^{M} a_k^{(a)} y_k. \tag{18}$$

A virtual beam without compression energy is used, so

$$U_c^{(a)} = 0. \tag{19}$$

Equations (18) and (19) can be now substituted into Eq. (15). At this stage, U_{tot} is defined as a polynomial of $(a_k^{(a)})_{k \in \{1,2...M\}}$ with all coefficients of degree less than or equal to 2. The extrema of the energy are determined by writing

$$\left\{ \frac{\partial U_{tot}^{(a)}}{\partial a_i} = 0 \right\}_{i \in \{1,2...M\}}. \tag{20}$$

Solving Eq. (20) makes it possible to determine coefficients a_i which will be put into Eq. (18) to obtain a particular solution y_a. It is worth noting that there is only one solution to this system (the degrees of the polynomials are limited to degree 2, the derivate has only one solution for each variable), whereas the real mechanism has several possible configurations.

2.4 Determination of the Equilibrium Solution on the Real System

The next step is to obtain the equilibrium solutions on the real system.

The particular solution derived from the previous equations is now used in Eq. (15). U_{tot} is a polynomial function of coefficients a_1 and a_2, each of these is present up to degree 4. Fig. 5 shows the shape of U_{tot} depending on coefficients a_1 and a_2.

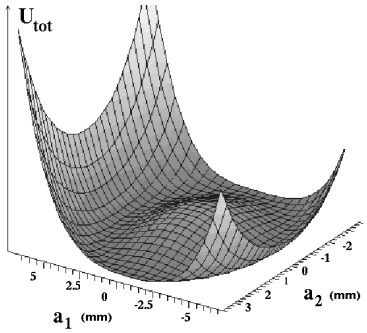

Figure 5. Energy of the system depending on coefficients a_1 and a_2, drawn for an external force of 10 N (central actuation).

By writing the equilibrium criteria of the real system, all the equilibrium shapes for a given external actuation are obtained (here for a given external force) as follows

$$\left\{ \frac{\partial U_{tot}}{\partial a_1} = 0, \frac{\partial U_{tot}}{\partial a_2} = 0 \right\}. \tag{21}$$

This is a system of two third order polynomial equations with several solutions. A numerical solver (the Maple© solver) is used to compute it.

For an external actuation force that is less than the snapping force, there are 5 equilibrium configurations, 2 of them are stable, 2 undefined (in sense of stability, *i.e.* stable for one variable and unstable for the other one) and one is unstable. Equation (4) is used to draw, as in Fig. 6, these 5 shapes. The five configurations were drawn for a centrally actuated beam as an example in Fig. 6. The unstable configuration, only using mode 1 is shown as shape *S1i*. The two stable configurations are shapes *S1p* and *S1m*, respectively for a positive and negative coefficient a_1. The two undefined solutions are shapes *S2p* and *S2m*, respectively for a positive and negative coefficient a_2. It is worthwhile noting that even if there are no higher modes than the first two modes in the latter equation, the upper modes still exist thanks to the particular solution. Finally, the force-displacement and the coefficients versus displacement curves can be drawn using Eq. (6), Eq. (13) and the result of Eq. (21).

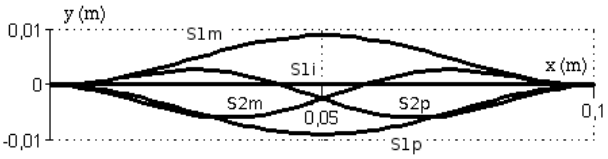

Figure 6. The five configurations of equilibrium for an actuation force of 10N, for a centrally actuated beam.

3 Performance Criteria

Several performance criteria (illustrated in Fig. 7) are defined for mechanism optimization. Some of these criteria are linked to stability positions (behaviour in a non-actuated state), others are linked to the behaviour of the system during a controlled switch from one position to the other.

We note P the normal force which would need to be applied to the structure in order to compress it from its initial length l_0 to the system length l without considering buckling. Hence, using the law of elasticity, P is determined by

$$P = SE\frac{l - l_0}{l_0}. \tag{22}$$

P should be compared with $P_c^{(2)}$ the critical buckling mode 2 load [11], given by

$$P_c^{(2)} = \frac{N_2^2 EI}{l^2}. \tag{23}$$

We define η_P as

$$\eta_P = \frac{P}{P_c^{(2)}}. \tag{24}$$

Very low values of precompression give a η_P that is lower than 1. In other words, the compressive force of the fully straight beam is smaller than buckling mode 2 critical force, so the system never uses mode 2 buckling. The *f-d* curve is only made of a branch *(b1)* using mode 1 buckling only, which is sinusoid shaped as in Fig. 7. It includes the 2 stable points and links them. As it only uses buckling mode

1, amplitude a_2 of Eq. (21) is always zero and it can be determined with the particular solution and amplitude a_2 set to zero in Eq. (21). In this case, the system switches in a fully straight configuration as in the case of shape *S1i* in Fig. 6 using only compression of the beam.

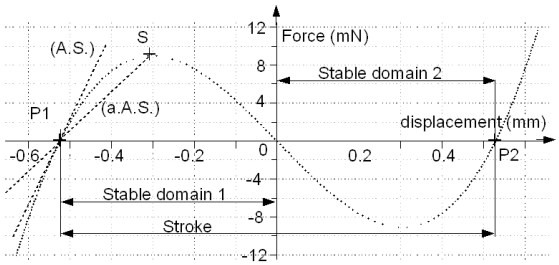

Figure 7. Performance indices: Switching point (S), apparent stiffness (A.S), average apparent stiffness (a.A.S) both on point P1, stroke and stable domains.

The case where η_P is higher than 1 with $P_c^{(2)}$ of the order of P has already been studied by M. Vangbo [12] for central actuation. In this case, a shape similar to Fig. 8 is obtained. There is still a mode 1 branch *(b1)* with a sinusoidal shape but it is cut by a *(b2)* negative stiffness branch. This branch uses mode 2 buckling and allows the system to shorten the branch *(b1)* lowering the force and the energy needed to switch from one stable position to the other. It is this way that mode 2 buckling helps the system to switch.

Concerning the branch *(b3)* due to the mode 3 buckling, the same behaviour as for the previous branch (b2) is obtained. It is an inverse stiffness branch with a higher absolute stiffness and it does not use mode 2 buckling (the two curves are fully independent). As it uses a higher mode, a higher level of energy is required and branch *(b2)* is always preferred over branch *(b3)* for single beam systems. However, in the case of double beam systems, amplitude a_2 of Eq. (21) is set to zero and branch *(b3)* is used. It is worth noting that there is a negative stiffness branch for every upper mode, which is not used for the same reasons. We do not integrate it into the model because all of the useful information is already included in the particular solution and it needs significant computing power to be solved.

If η_P is greatly larger than 1, as in our simulations and experiments (we have $P = 30000$ N and $P_c^{(2)} = 161$ N, hence $\eta_P = 186$), the shape of branch *(b1)* is changed to become closer to the particular solution curve, which is a positive stiffness line as seen in Fig. 9. It still links continuously the two stable positions. The branch *(b2)* still exists, even if it does not appear in the graph since it is completely flattened. Hence the branch *(b1)* is directly cut by the branch *(b2)* (as seen in Fig. 11) and the two portions of the branch *(b1)* seem vertical. Moreover, the vertical portion of branch *(b1)* around the zero displacement point still exists and appears in all the following *f-d* curves, as they are simply cut to the useful force range.

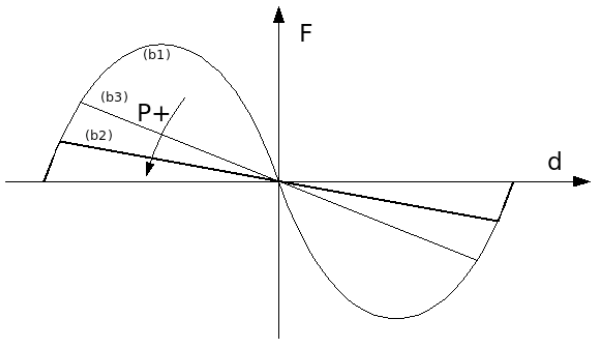

Figure 8. f-d curve for a central actuation depending on parameter P.

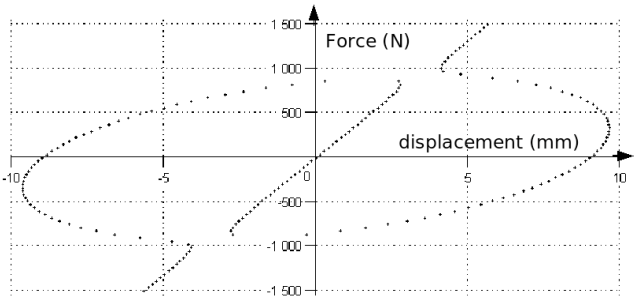

Figure 9. Full range f-d curve for a central actuation with a high η_P parameter ($\eta_P = 42$, used from the following simulations). The positive stiffness line appears representing the particular solution behaviour. The actual f-d curves are obtained by cutting this curve to the useful force values, here $F = -40$ N to $F = 40$ N as in Fig. 11.

For a shifted actuation, the branch is using both mode 1 and mode 2 buckling in a non-obvious way. It is not possible to use as for a central actuation an analysis with a branch for each mode behaviour. It is one of the point of this paper to propose a model which directly incorporates mode 1 and mode 2 buckling, without needing a branch split as do previous works. Still, η_P is representative of the importance of mode 2 buckling during the switch.

It should be noted that increasing P also increases the non-linearities of the mechanism and at a certain point, a model which takes into account the geometrical non-linearities, such as elliptic displacements [5], is needed.

We also consider the switching point, the point where the applied force reaches its maximum. We take into consideration both the maximum applied force F_{max} (therefore the maximum force needed to switch from one position to another) and its position (which delimits the domain that can be used in non-actuated state, *i.e.* the depth of the stable domain).

We use the apparent stiffness and the average apparent stiffness which represents the stiffness on the stable point and the average stiffness from the stable point to the switching point, respectively. These are key parameters to qualify the rigidity of the system.

The actuation stroke should also be studied along with the depth of the two stable domains.

4 Simulation Results

First, a bistable structure with a centred force is investigated. This actuation does not involve mode 2. The force is then shifted to determine the effect of a translation of the actuator.

A beam of length 100 mm, width 20 mm and thickness 0.4 mm is used in a 304 stainless steel of Young modulus E=187.5 GPa and the beam is subject to a 2% precompression for the computation and experimental tests.

4.1 Bistable Beam with a Central Actuation Force

For this system, a precompression such as P is higher than $P_c^{(2)}$ is selected.

Fig. 10 represents the chronology of the switching. A central force (2) is applied up to a certain force when the beam buckles in mode 2 (3). Note that there are two symmetrical possible shapes with equal probability [9] depending on the sign of a_2. Then we switch and go to (4) where the beam comes back to a mode 1 only buckled shape.

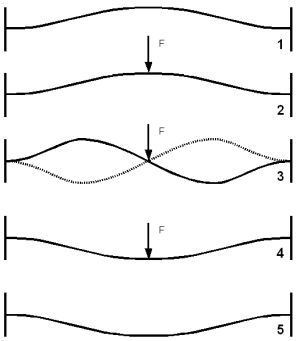

Figure 10. Snapping sequences for a typical clamped-clamped beam. Mode 2 buckling is used to help the switch from one position to the other.

The *f-d* curve is shown on Fig. 11. A classical *N-shape* is obtained, *i.e.* there is a constant negative stiffness around the zero displacement point. There are several branches on this graph.

The branch (*b1*) represents the straight configuration. It is sinusoidal shaped and is cut in the diagram as it goes very high. In Fig. 10, this branch is used on configurations 1, 2, 4 and 5. This branch only uses buckling mode 1, *i.e.* the coefficient a_2 along this branch is zero.

Branches (*b2p*) and (*b2m*) use buckling mode 2. These branches only appear when normal compression is high enough to obtain buckling mode 2, so they only exist for a restricted domain. In this domain, the entire energy of the system is lower in the case of buckling mode 1 and mode 2 than in the case of mode 1 buckling only so one of these

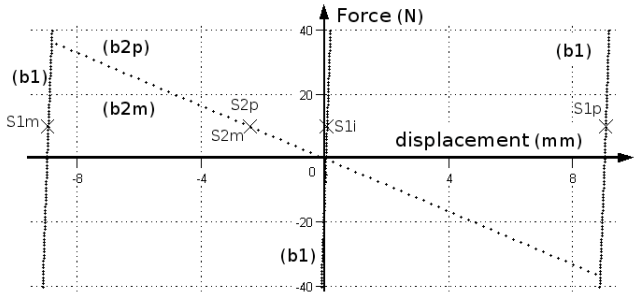

Figure 11. *f-d* curve for a central actuation clamped-clamped beam.

branches is preferred. In the *fn-d* curve (Fig. 12), it can be observed that the two (*b2*) branches exist when the normal force is equal to the critical force of the second buckling mode [1]. These branches have the same probability and one of those is chosen by the system.

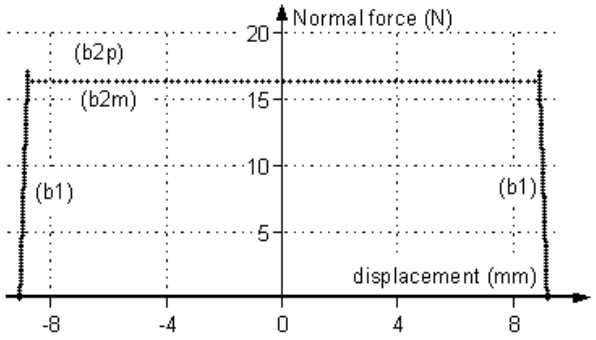

Figure 12. *fn-d* curve for a central actuation clamped-clamped beam.

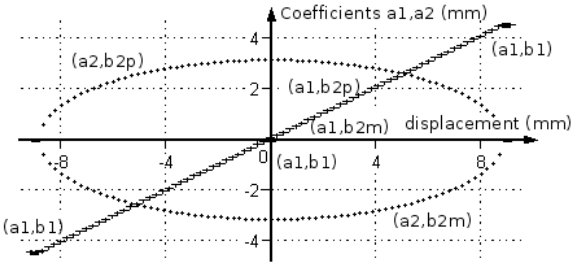

Figure 13. Coefficients a_1 (cross) and a_2 (circles) versus displacement curves for a central actuation clamped-clamped beam.

In Fig. 13, the evolution of the coefficients a_1 and a_2 is represented. Displacement is proportional to coefficient a_1. The coefficient a_2 curve is an ellipsoid with two separate upper (*b2p*) and lower (*b2m*) branches. At the two extreme positions, the a_2 coefficient is zero.

In Fig. 6, the five possible configurations found for a 10 N actuation are drawn. The three mode 1 shapes are

S1m, *S1i* and *S1p*, the negative state, the unstable straight configuration and the positive state shapes of branch (*b1*), respectively. Buckling mode 2 shapes *S2m* and *S2p* belong to branches (*b2m*) and (*b2p*), respectively.

In such systems, the apparent stiffness is excellent (120 kN/m) and the maximum force quite high (37 N). The stroke is the maximum which can be obtained with this mechanism. On the other hand, the width of the stable domain is only half of the stroke.

4.2 Bistable Beam with a Shifted Actuation Force

A shifted force actuation is now used (as in Fig. 14). This breaks the symmetry *i.e.* whereas only odd modes are excited in the case of a central force, all modes came actuated there.

Fig. 14 presents a schematic chronology of the snapping process. The snapping is delayed compared to a central actuation. The system parameters are the same as for a central actuation (see Fig. 1), except that the actuator has been shifted laterally.

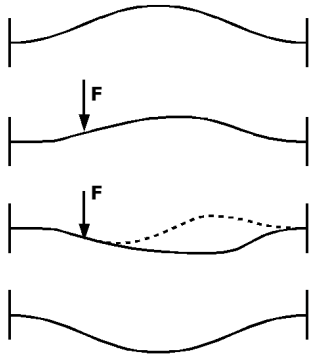

Figure 14. Switching sequences with a shifted force actuator, the snapping is delayed.

The previous theoretical model was used with x_F changed to 40% in Eq. (14). The particular solution was recalculated and now a combined mode 1 and mode 2 actuation appears (plus upper modes). The resulting *f-d*, *fn-d* and coefficients versus displacement curves are drawn in Fig. 15, Fig. 17 and Fig. 18, respectively. The full *f-d* curve (before cutting) is given in Fig. 16.

The *f-d* curve indicates a rounded curve with two separate branches, (*b2p*) and (*b2m*), and a hysteresis. The straight configuration still exists and links the two branches (this is out of the range of the curve and is not displayed in the normal *f-d* curve, however, it appears in Fig. 16).

The plateau of the critical mode 2 now does not appear on the *fn-d* curve. This is due to the combined mode 1 and mode 2 actuation.

The curves of both coefficients a_1 and a_2 exhibit a more complex shape than in the case of a central actuation. Coefficient a_2 starts to increase immediately after the stable position. More importantly, there is no continuity between the

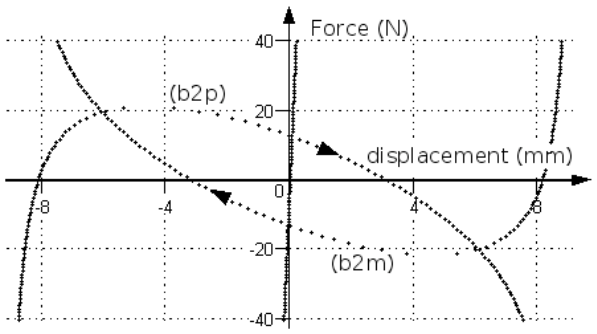

Figure 15. *f-d* curve for a clamped-clamped beam with a shifted (40%) actuation.

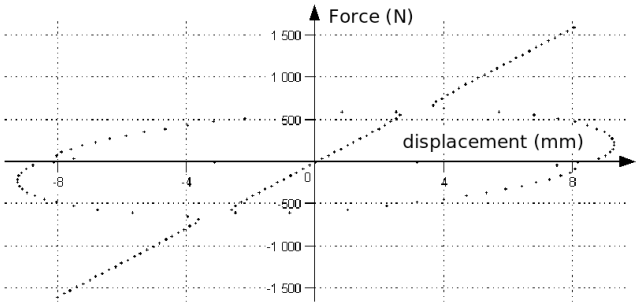

Figure 16. Full range *f-d* curve for a shifted (40%) actuation

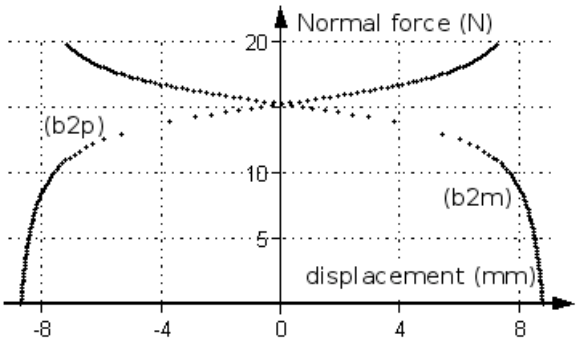

Figure 17. *fn-d* curve for a shifted actuation clamped-clamped beam.

two branches (except with the unstable straight branch). This means that the delayed snapping corresponds to a branch jump. It cannot be accurately predicted with a static model. Moreover, this branch jump will be very sensitive to small machining tolerances and is hardly predictable.

Concerning the performance of this system, the maximum force (25 N) has decreased compared to the central actuation one, the apparent stiffness has fallen to 24500 N/m and the stroke is smaller (16.3 mm compared with 18 mm).

4.3 Use of more than 2 modes of buckling

In order to verify the hypothesis that only the first two mechanically compatible modes are involved (modes 1 and

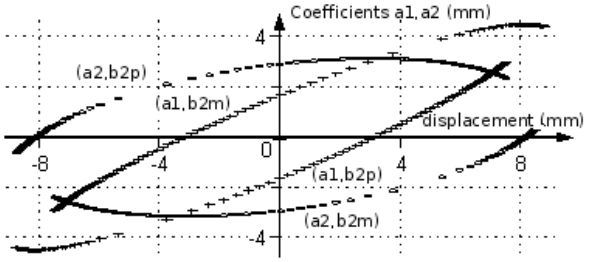

Figure 18. Coefficients a_1 (cross) and a_2 (circles) versus displacement curves for a shifted actuation clamped-clamped beam.

2 for a single beam, modes 1 and 3 for a double beam), a system with the three first modes (*i.e.* mode 1, mode 2 and mode 3) is investigated.

Mode 3 buckling is defined as

$$y_3 = a_3 \left(1 - \cos\left(4\pi \frac{x}{l}\right)\right). \tag{25}$$

The deflection y is now written as

$$y = y_1 + y_2 + y_3 + y_a \tag{26}$$

where y_1, y_2 and y_3 are defined by Eqs. (1), (2) and (25).

The equilibrium equations are now changed into

$$\left\{ \frac{\partial U_{tot}}{\partial a_1} = 0, \frac{\partial U_{tot}}{\partial a_2} = 0, \frac{\partial U_{tot}}{\partial a_3} = 0 \right\}. \tag{27}$$

As an example, a central actuation *f-d* curve is drawn in Fig. 19. It appears that the curve has the same shape than the previous one with a_1 and a_2 (branches (*b1*), (*b2m*) and (*b2p*)), plus two superposed branches that use only buckling mode 1 and mode 3 (branches (*b3m*) and (*b3p*) with $a_2 = 0$ for these branches). So that *f-d* curve is a superposition of the previous curve using buckling mode 1 and mode 2 and another one using only buckling mode 1 and mode 3 (actually the double beam *f-d* curve). This is a consequence of the orthogonality of the modes. This result was already previously demonstrated by J. Qiu *et al.* [8] and M. Vangbo [12] with other methods and is still valid for a shifted force. This is explained with the present model and the use of a particular solution, only the first two modes are important for the buckling modelling as the mechanism cannot simultaneously use three modes. Consequently, only the first two modes are needed in the general solution to model a bistable switch.

4.4 Using a Pre-Shaped Beam

Pre-shaped beams, as used by J. Qiu [8], make it possible to obtain monolithic bistable mechanisms which are manufactured directly by cutting into a single material part such as silicon wafers. The model has been explained in the publication referred above and this section is intended to show

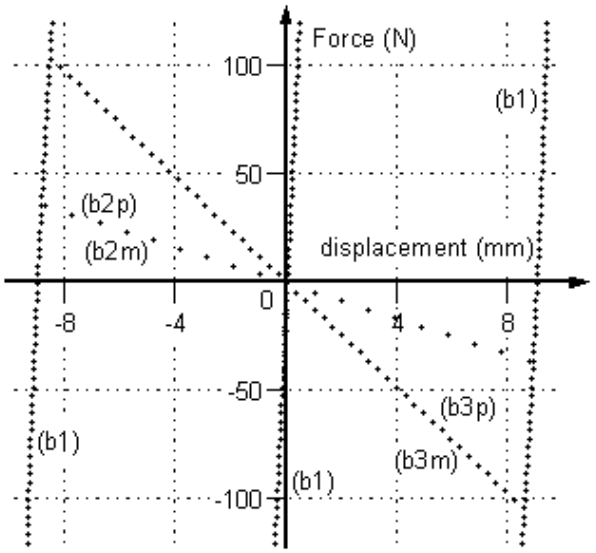

Figure 19. *f-d* curve for a central actuation beam with 3 free parameters a_1, a_2 and a_3.

how the present model can be extended to take into account the specificities of this type of bistable system.

Pre-shaped beams are based on the use of a beam which already has a non-straight shape when relaxed, typically the sinus mode 1 buckling shape. Hence, the free length is no longer l_0 but the length of the relaxed system calculated using the same formula as for the beam of current length $\bar{s}$ in the free length $\bar{s_0}$ is therefore defined as

$$\bar{s_0} = \int_0^l ds = \int_0^l \sqrt{1 + y_0'(x)^2}\, dx \tag{28}$$

with y_0 the shape of the beam when relaxed, either mode 1 buckling or any shape. $\bar{s}$ (from Eq. (11)) is unchanged. Then Eq. (9) becomes

$$\varepsilon = \frac{\bar{s} - s_0}{s_0}. \tag{29}$$

Furthermore, the bending energy needs to be changed to take into account the initial shape, so Eq. (8) is now replaced by

$$U_b = \frac{EI}{2} \int_0^l (y''(x) - y_0''(x))^2\, dx. \tag{30}$$

This makes the system not symmetric in behaviour. The latter equation can also be used to take a predeflection of stratified structures into account both in the case of a passive or an active structure [6]. No tests were carried out for it in this work so the simulation results are not presented. However, since it uses the same approach as J. Qiu's work, it is expected to produce good results.

5 Experimental Validation

Experimental validations were carried out to validate the model. We used the test bench shown in Fig. 20.

The bistable beam is made of stainless steel 304, with a Young modulus of E=187.5 GPa, length 100 mm, width 20mm and thickness of 0.4mm as in the case of the simulation.

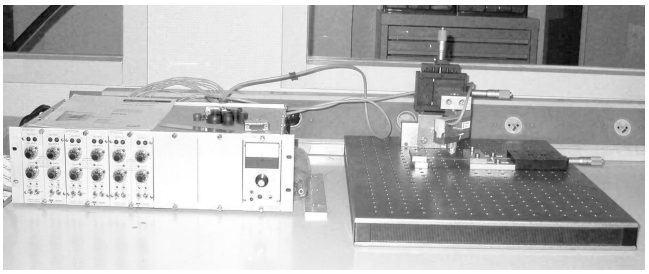

Figure 20. Test bench for force-displacement measurement. On the left is the Vishay console, on the right is the mechanical setup.

The 2% precompression (hence a 2 mm displacement in the left direction) is obtained through the use of a Thorlabs PT1 travel translation table featuring a 10 μm adjustment. The precompression chosen was small enough to stay in the small-assumption hypothesis and to avoid plastification. Since plastification also occurs due to dynamical effects when switching, it was not possible to calculate a maximum precompression without plastification. The beam was checked after the test to ensure that no plastification occurred.

Force is applied through a setup with two PT1 translation tables. One is used to set the position of the force application (horizontal displacement). The other controls vertical displacement, hence, the displacement as defined in all *f-d* curves. It can be observed that the translation table is reversed compared to the classical Thorlabs setup, so the down-face of the vertical table is seeable in Fig. 20. This particular setup was made since the Thorlabs table uses springs and a precision micrometer. The up-face of the table is pressed to the micrometer. This setup makes it possible to ensure the system force is locked by the micrometer instead of the springs ensuring good contact and therefore optimal precision.

The force is measured through an HBM S2-600 force sensor (an S-shaped force sensor with an internal double Wheatstone bridge) interfaced with an analogic Vishay Wheatstone bridge console, a setup said to give a 4 digit precision. The force sensor was calibrated before the tests which confirms a degree of accuracy greater than 0.04 N.

Next, the force is applied to the beam via a special plastic-made V-shaped shaft. With such a system, only a negative force can be applied but we avoid friction and damping effects.

Experiments were performed for the two simulation cases presented above. Central and shifted (40%) force actuation are superposed to the simulation curves in Fig. 22 and Fig. 23, respectively. For each experiment, we show the mean values of ten measurements. The experimental points show that the model has a high degree of accuracy for the shape of the *f-d* curves. The displacement appears to be overestimated by roughly 5% in every simulation. The level of forces is always lower than expected for these experiments but there is an uncertainty concerning the Young modulus material although the global shape seems fine. In the case of central force actuation, the vertical branch of the N is rotated, an effect which seems due to the limit of the model in this case, since a fully vertical branch cannot be obtained in the real world.

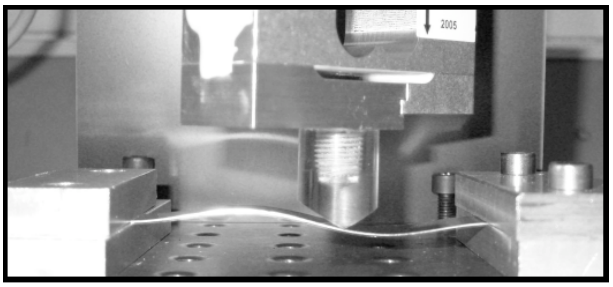

Figure 21. Test bench for force-displacement measurement.

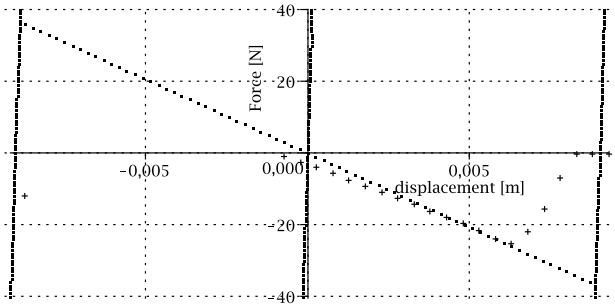

Figure 22. *f-d* curve for a central actuation clamped-clamped beam, with experimental points in cross.

As explained before, another effect are hysteresis phenomena. There is a small hysteresis due to the two branches (branch (*b2p*) and branch (*b2m*)) for a shifted force actuation. There is also a smaller hysteresis phenomenon on each branch. This effect was observed on a nylon double beam system [9]. It was not predictable using the proposed elastic model. It is observed on the central actuation *f-d* curve (Fig. 22). The null force is achieved for a displacement of about 0.85 mm (5% of the stroke, giving a 10% hysteresis).

To emphasize the hysteresis, an experiment using the same conditions of a shifted force actuation as in Fig. 15 has been performed. The same stainless steel has been used but from another set of steel plate from the same provider. The branch is followed by applying a displacement to be close

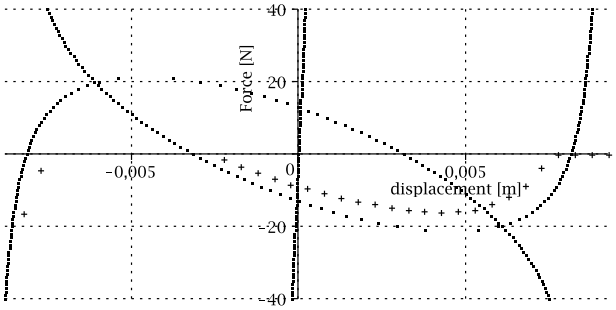

Figure 23. *f-d* curve for a shifted (40%) actuation clamped-clamped beam, with experimental points (cross).

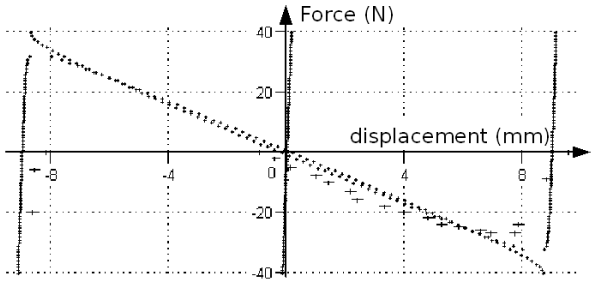

Figure 25. *f-d* curve for a clamped-clamped beam with a slightly shifted (49.5%) actuation, with central actuation experimental points (cross).

to the point where the force becomes positive, then coming back. The results are shown in Fig. 24. This experimental protocol ensures sticking to the same branch during actuation and a branch hysteresis effect is observed.

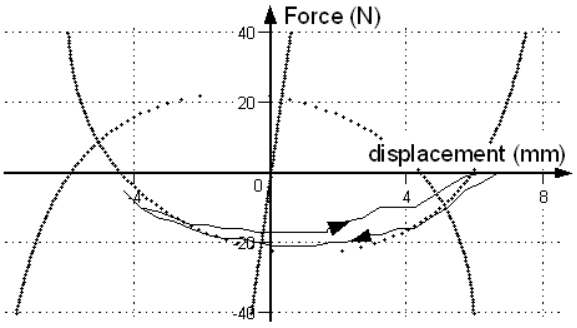

Figure 24. *f-d* theoretical curve with a 40% actuation shift (points), compared to experimental measurements (line).

6 Discussion of Results

The aspect of the *f-d* curve obtained with a shifted actuation has a high degree of consistency with the experimental data. However, the *N-shape* obtained for a central actuation seems less accurate. Actually, central actuation is a very special case of actuation (no actuation on the second buckling mode). This causes the transition between branches (*b1*) and (*b2m*) or (*b2p*) to be abrupt whereas a smoother transition would be physically more acceptable. A model with a very small shift has been implemented. The resulting *f-d* curve of a closely central actuation (force is applied at 49.5% of the length) is presented in Fig. 25 using the shifted actuation equation previously presented. Experimental data taken from a central actuation test with the second set of steel is shown on the same curve.

Using a small shift in the actuation position results in a very small hysteresis and a smoother transition. The latter is much better but the apparent stiffness is still overestimated. This could be a consequence of the linearity of the model. Although not shown there a lower precompression leads to a better agreement of the theoretical with the experimental data. This means that the linear model is no longer valid for high level of precompression where non-linearities should be accounted for. Concerning hysteresis, even if there is currently hysteresis in the real system, the hysteresis exhibited by the model seems to be too low to explain the actual phenomenon.

The snapping location, *i.e.* the point where the applied force becomes negative, has a major impact on the behaviour of the system. This point indicates the end of the stable domain. After it, the system does not return automatically to its first position. Furthermore, it delimits the domain where the actuator is active. For a central actuation beam, due to the *N-shape* of the *f-d* curve, the stable domain is half of the stroke of the system. In the case of shifted actuation, the hysteresis increases the stable domains. In this configuration, we can inject energy in a longer stroke. Since the total energy to put into the system is relatively constant for a reasonably shifted force (from 50% to 65% of length, the energy increases by less than 15%), the maximum force decreases. It has been demonstrated in the previous example that there has been a 37 N to 21 N decrease in the peak force, a 43% drop. Furthermore, due to the cantilever effect, the stroke of the actuator decreases even if the active stroke increases. Another advantage is the rise of the stable domain. The system has increased robustness against displacement disturbance.

Another way to illustrate this change is to use an energy-based method. As mentioned before, the effective snapping energy is quite constant but the actuator is not designed for this energy. It is actually designed, in most cases, to exceed the maximum required force and stroke so a design energy can be defined as the product of the stroke and the maximum force of the actuator. Then the ratio effective switching energy over the design energy can be considered. This has been represented in Fig. 26 for a central actuation and for a shifted (40%) actuation in Fig. 27. It can be seen that this ratio is only 25% for the central actuation (due to the triangular-like *N-shape*) and increases significantly for a shifted actuation (roughly 50%-60%). This means that the actuation is best used with a shifted force so it is possible to choose more compact actuators.

It is worth noting that the opposite effect is obtained

when the actuation is shifted too far from the center. Indeed, a high proportion of the energy is transmitted in the third and higher modes. This energy is not used directly in the snapping dynamic and is mainly lost. This leads to an increase of the maximum force in the case of significantly shifted actuation.

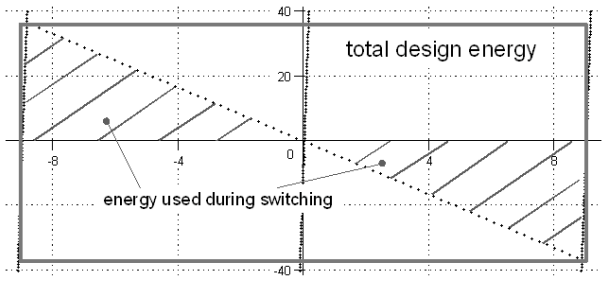

Figure 26. Energy used and actuator total energy for a central actuation clamped-clamped beam. The ratio is about 25%.

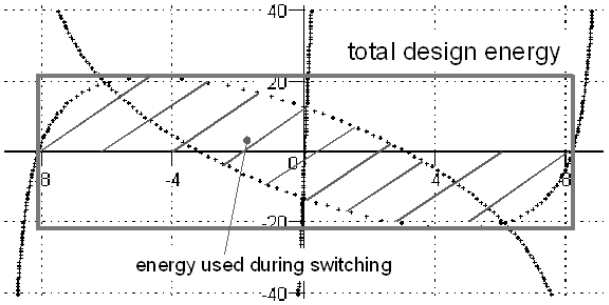

Figure 27. Energy used and actuator total energy for a shifted (40%) actuation clamped-clamped beam. The ratio is much increased compared with the central actuation.

Although shifted actuation seems very useful, there are some problems. This type of actuation reduces the stroke, the apparent stiffness and average apparent stiffness which are key parameters for evaluating the performance of a bistable mechanism. It is also worth noting that the actuation point will rotate during actuation, which could cause difficulties for a monolithic design (instead, the central actuation double beam mechanism avoids rotation of the central point). Another problem is that during snapping, a shifted actuation mechanism will jump from one stable branch to another leading to harsh shocks in the structure. Instead, the central actuation mechanism has a much smoother continuous deflection.

Finally, on one hand, the central force actuation seems very good in terms of stability, having good apparent stiffness, maximum stroke for the system and a high maximum force. On the other hand, shifted actuation makes it possible to use the actuator in a much more efficient way.

Smart use of both phenomena would include actuation using a shifted force and a static use of the two stable positions that benefits from both the stroke and the apparent stiffness of a central actuation. If a design can accept rotation of the central point, a single bar system can be used instead of the double beam system. For such a mechanism, a different actuation location can be used to lower the maximum force and the stroke of the actuator, two parameters that imply a reduction of the necessary actuator size. It means that the system has very different behaviour according to the point of force application. Splitting the input and output locations should be considered for such bistable systems.

7 Conclusion

We have proposed a method that makes it possible to calculate the behaviour of most buckled-beam based bistable mechanisms actuated with normal force. We have demonstrated that deflection can be split into the first two modes, which have complex behaviour, and upper modes which are simply related to equilibrium.

Most bistable mechanisms of the compressed beam class are actuated in their central point to obtain a maximum stroke, this is a mode 1 actuation. We have shown that a combined mode 1 and mode 2 actuation can also be of value (lower snapping force, longer stable domain…) and should be considered for a mechanical design. Using separate input and output makes it possible to benefit from different behaviour of the same structure.

Experimental validations were carried out and demonstrated that this model provides rather good results. Using the previous method, we were able to simulate a very low shift (0.5%) from the central location on the structure. It appears that this simulation gives a more accurate model.

We have shown that an optimal choice of the actuator location can lead to a significant decrease of the power needed by the actuator. This makes it possible to use more compact actuators without modifying the performances of the system.

References

[1] M.P. Brenner, J. Lang, J. Li, J. Qiu and A. Slocum. Optimal design of a bistable switch. *Proc. Natl. Acad. Sci*, **100**(17), 9663–9667, 2003.

[2] P. Cazottes, A. Fernandes, J. Pouget and M. Hafez. Optimisation de mécanismes bistables : structures et actionneurs. *In 18ème Congrès Français de Mécanique (CFM07)*, Grenoble, France, 27-31 Aug. 2007.

[3] M. Hafez, M.D. Lichter and S. Dubowski. Optimized binary modular reconfigurable robotic devices. *IEEE/ASME Transactions on Mechatronics*, **3**(1), 18–25, March 2003.

[4] B.D. Jensen and L.L. Howell. Bistable configurations of compliant mechanisms modeled using four links and translation joints. *Journal of Mechanical Design, Transaction of the ASME*, **126**, 657–666, July 2004.

[5] B.D. Jensen, L.L. Howell and L.G. Salmon. Design of two-link, in-plane, bistable compliant micro-

mechanisms. *Journal of Mechanical Design, Transaction of the ASME*, **121**, 416–419, September 1999.

[6] H. Matoba, T. Ishikawa, C.-J. Kim and R.S. Muller. A bistable snapping microactuator. *In Proceedings of the IEEE Workshop on Micro Electro Mechanical Systems (MEMS 94)*, Oiso, Japan, 25-28 Jan. 1994.

[7] J. Qiu. *An Electrothermally-Actuated Bistable MEMS Relay for Power Applications*. PhD thesis, Department of Mechanical Engineering, Massachusetts Institute of Technology, 2003.

[8] J. Qiu, J.H. Lang and A.H. Slocum. A curved-beam bistable mechanism. *Journal of Microelectromechanical Systems*, **13**(2), 137–146, April 2004.

[9] T. Schiloer and S. Pellegrino. Multiconfiguration space frames. *In Structures, Structural Dynamics and Materials Conference, AIAA 2004-1529*, 19-22 April 2004.

[10] M. Shahinpoor, Y. Bar-Cohen, J.O. Simpson and J. Smith. Ionic polymer-metal composites (ipmcs) as biomimetic sensors, actuators and artificial muscles - a review. *Smart Materials and Structures*, **7**, 15–30, 1998.

[11] S.P. Timoshenko and J.M. Gere. *Theory of elastic stability*. (McGraw-Hill, 2nd edition, 1961).

[12] M. Vangbo. An analytical analysis of a compressed bistable buckled beam. *Sensors and Actuators*, **69**, 212–216, 1998.

[13] M. Vangbo and Y. Bäklund. A lateral symmetrically bistable buckled beam. *Journal of Micromechanics and Microengineering*, **8**, 29–32, 1998.

[14] G. Wang and M. Shahinpoor. Design, prototyping and computer simulations of a novel large bending actuator made with a shape memory alloy contractile wire. *Smart Materials and Structures*, **6**, 214–221, 1997.